Faired Towline Hydrodynamics

D. E. CALKINS*
Naval Undersea Research and Development Center, San Diego, Calif.

A theoretical analysis for determining the hydrodynamic forces on a faired towline is developed. The analysis requires that the hydrodynamic forces acting on an element of the towline be defined as a function of the towlines local inclination angle to the flow, and of the Reynold's number. These hydrodynamic forces are known as loading functions. The analysis is based on consideration of the boundary layer formed on the airfoil shaped cross section used for the towlines. The Reynold's number effect on the loading functions is derived using momentum theory, and requires that the pressure distribution around the airfoil section be defined. Potential flow theory is used, and gives excellent results when compared with pressure distribution measurements made on models. The theoretical loading functions are compared with model data obtained from water channel, tow tank and wind-tunnel tests. The analytical results show excellent correlation with the data. The analysis has been termed Boundary-Layer Loading Functions (BLLF).

Nomenclature

b = towline span length = unit length
c = towline chord length
C_R = total drag coefficient (R/qS)
$F(\phi)$ = normal force/unit length
$G(\phi)$ = tangential force/unit length
H = shape factor (δ^*/θ)
K = mixed momentum thickness correction factor
q = dynamic pressure ($\frac{1}{2}\rho U^2$)
R = normal force/unit length ($\phi = 90°$)
Re = Reynold's number ($U_\infty c/\nu$)
S = reference area based on either chord c, or thickness t where length b is taken to be 1 ft
t = towline thickness length
t/c = towline thickness/chord ratio
u = velocity in the boundary layer along X axis
u = velocity in airfoil wake parallel to the direction of motion
U = velocity outside of the boundary layer along X axis
U_∞ = freestream velocity
U_0 = chordwise velocity ($U_\infty \sin\phi$)
v = velocity in the boundary layer along Z axis
V = velocity outside of the boundary layer along Z axis
V_0 = spanwise velocity ($U_\infty \cos\phi$)
x = distance along towline chord
y = distance normal to xz plane
z = distance along towline length
δ = boundary-layer thickness
δ^* = boundary-layer displacement thickness, $\int_0^\infty \left(1 - \frac{u}{U}\right) dy$
θ = boundary-layer momentum thickness, $\int_0^\infty \frac{u}{U}\left(1 - \frac{u}{U}\right) dy$
θ_{zx} = cross-momentum thickness, $\int_0^\infty \frac{u}{V}\left(1 - \frac{u}{V}\right) dy$
ν = fluid kinematic viscosity
ρ = fluid density
τ = shearing stress
ϕ = local towline angle measured from horizontal

Subscripts

le = leading edge
te = trailing edge
tr = transition location
∞ = infinity

Presented as Paper 69-753 at the CASI/AIAA Subsonic Aero- and Hydro-Dynamics Meeting, Ottawa, Canada, July 2–3, 1969; submitted July 18, 1969; revision received March 11, 1970.

* Head, Hydromechanics Program, High Speed Towed Sonar Branch. Member AIAA.

1.0 Introduction

ADVANCED faired towlines, developed by the aerospace industry for the U. S. Navy, have successfully demonstrated improved performance over existing designs.

The Boeing Company configuration may be described as a continuous integral design, Fig. 1. The strength member is a molded fiber glass shape which is contoured to the airfoil section. A flexible rubber trailing edge is bonded to the strength member to provide the aft contour of the airfoil. The design utilizes an NACA 63A022 section.

The second design was originated by M. Kramer, who further developed it while a consultant for North American Aviation. The design, Fig. 1, consists of rigid, articulated links which are 4 ft in length. The strength member is 17-4 PH stainless steel with an extruded polypropylene aft fairing. The section is an NACA 0020 airfoil.

These designs have had a limited evaluation in a series of towing trials so that some indication of the potential drag reduction they offer is available. The results are summarized in Table 1. Eames[1] summarizes frontal area drag coefficients for other types of fairings which have been used in conjunction with stranded steel cables. Table 2 compares the drag coefficients of these fairings with that of the basic cable. The degree of drag reduction offered by the advanced faired towlines is obvious.

Proper performance optimization of these towlines requires a theoretical analysis which would be sensitive to various section shapes so that, for example, studies could be conducted which would compare the drag characteristics of NACA "laminar flow" airfoils with those of sections designed for full turbulent flow. The relatively low Reynold's numbers at which these designs operate play an important part in the performance analysis because of separation effects.

2.0 Towed System Analysis

The performance analysis of a towed system results in both the spatial configuration and the tension distribution. The important parameters which are considered are shown in Fig. 2. The inputs necessary for this analysis (Fig. 3) are

Table 1 Advanced towline frontal area drag coefficients

Towline	C_R
Boeing	0.053
North American	0.067

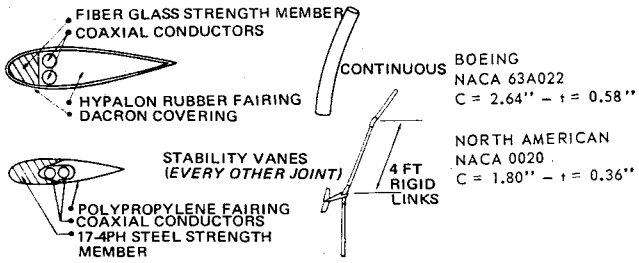

Fig. 1 Faired towline details.

1) the normal ($\phi = 90°$) drag coefficient as a function of Reynold's number, 2) the variation in the nondimensional normal loading function $F(\phi)/R$ with the local towline angle ϕ, and 3) the variation in the nondimensional tangential loading function $G(\phi)/R$ with the local towline angle ϕ.

Several authors have developed theories on the relationship between the normal and tangential forces (loading functions) and their variation with the local towline angle. The most widely quoted are Eames,[1] Clark,[2] and Whicker.[3] None of the theories have approached the problem from pure boundary-layer considerations, hence the effect of Reynolds number is not directly taken into account.

3.0 Normal Force

It was decided to approach the problem of defining the loading functions by examining the boundary layer developed on the surface of the faired towline. The analysis is based on swept wing theory which has been validated by experiment.

The following assumptions were made concerning the scope of the analysis: 1) the towline section is uncambered, 2) the chord and thickness ratio are constant in the spanwise direction (along the towline), 3) there are no discontinuities along the towline, 4) the angle of yaw is zero; i.e., no side forces are considered, and 5) the boundary layer is not separated in either the laminar or turbulent region.

3.1 Momentum Drag

Consider the two dimensional flow past the foil section shown in Fig. 4. The flow pressure is constant in the fluid field except in the boundary layer and in the wake, which are shown shaded. Starting from the stagnation point, *le*, boundary layers are present on the upper and lower surfaces of the foil. Boundary layers are generally laminar for some

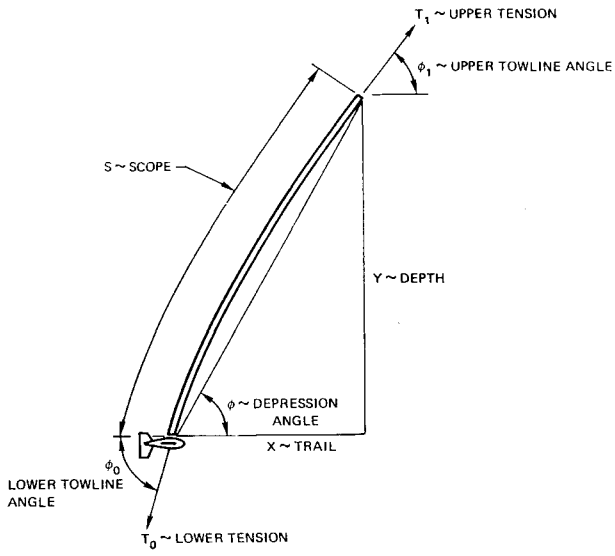

Fig. 2 Towed system.

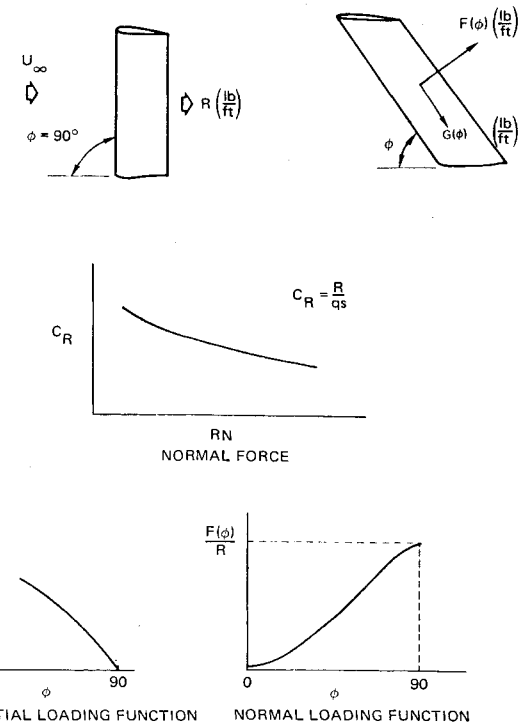

Fig. 3 Towline analysis.

distance aft to transition which occurs at the point x_{tr}. After a transition region, fully turbulent boundary layers are formed to the trailing edge *te*. The boundary layers of the upper and lower surface coalesce to form a wake which extends downstream to infinity.

The wake has a minimum thickness a short distance downstream of the trailing edge and then becomes gradually broader. Static pressure in the wake is greatest at the trailing edge and decreases downstream. The static pressure in the wake eventually becomes equal to the static pressure of the freestream. For a section of the wake sufficiently downstream for this to be true, it is easy to show from momentum considerations (Ref. 4) that the normal force R per unit length is

$$R = \rho \int_{-\infty}^{\infty} u(U_0 - u)\, dy \tag{1}$$

$$R = C_R \tfrac{1}{2} \rho U_0^2 tb = C_R \tfrac{1}{2} \rho U_0^2 t \tag{2}$$

The momentum thickness of the wake far downstream θ_∞ is defined as

$$\theta_\infty = \int_{-\infty}^{\infty} \frac{u}{U_0}\left(1 - \frac{u}{U_0}\right) dy \tag{3}$$

so that

$$C_R = \frac{2.0}{t} \int_{-\infty}^{\infty} \frac{u}{U_0}\left(1 - \frac{u}{U_0}\right) dy \tag{4}$$

The momentum thickness θ_∞ may now be evaluated in terms of the momentum thickness at the trailing edge of the foil θ_{te}.

$$\theta_\infty = \theta_{te}\, (U_{te}/U_0)^{(H_{te} + 5)/2} \tag{5}$$

Table 2 Faired cable frontal area drag coefficients

Towline	C_R
Bare cable	1.20
Trailing fairing	0.30
Sectional fairing	0.20

If a value of $H_{te} = 2.0$ is used, according to Thwaites,[5] Eq. (4) becomes

$$C_R = 2.0/(t/c)[(\theta_{te}/c)^{6/5}\ (U_{te}/U_0)^{21/5}]^{5/6} \quad (6)$$

where θ_{te} is the sum of the momentum thicknesses on the upper and lower surfaces.

The momentum thickness θ_{te} is dependent on the extent of both the laminar and turbulent boundary layers and may be evaluated according to Thwaites[5] as

$$C_R = \frac{2.0}{t/c}\left[\frac{1.422}{Re^{3/5}}\left\{\frac{U_{te}}{U_0}\int_0^{x_{tr}/c}\left(\frac{U}{U_0}\right)^5 d\left(\frac{x}{c}\right)\right\}^{3/5} + \frac{0.02429}{Re^{1/5}}\int_{x_{tr}/c}^{1.0}\left(\frac{U}{U_0}\right)^4 d\left(\frac{x}{c}\right)\right]^{5/6} \quad (7)$$

The computation of the normal force requires the potential solution for the velocity ratio U/U_0 over the two-dimensional section. Several methods are available for this solution. However, one which is particularly attractive and was used successfully is that developed by Weber.[6]

3.2 Boundary-Layer Transition Location

The determination of the location of the boundary-layer transition is at best a difficult problem even in the two-dimensional case. It generally is true that 1) transition occurs near the minimum pressure point and 2) transition moves toward the trailing edge with decreasing Reynold's number.

However, it has been observed by Gregory, Stuart, and Walker[7] that in the three-dimensional case, transition moves forward with increasing sweep angle. This trend would therefore seem to contradict the previous statement 2. In addition, the ambient stream turbulence level will affect transition causing it to occur nearer to the leading edge as the level increases in intensity.

Since time did not allow for a more thorough analysis of the transition location, it was decided to use experimental data from Silverstein and Becker[8] that were obtained on a series of NACA 4-digit airfoil sections. The transition location (Fig. 5) is shown for three thickness/chord ratios as a function of Reynold's number. The curves were extrapolated over the lower Reynold's number range.

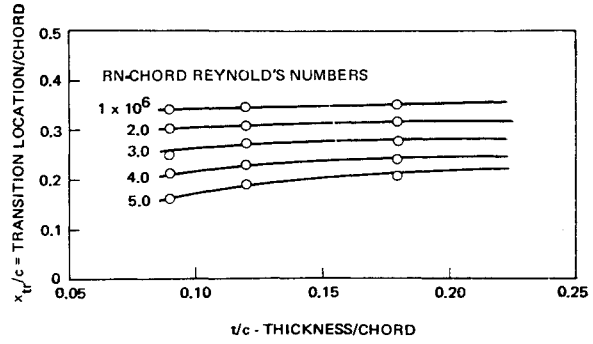

Fig. 5 Transition location NACA-4 digit series section.

4.0 Loading Functions—$F(\phi)$ and $G(\phi)$

It has been theorized by Jones[9] that the pressure forces on a swept wing of constant chord are determined solely by the component of velocity normal to the leading edge. This has been verified experimentally by Lippisch and Beuschausen[10] and Danneberg.[11]

The investigations of Jones[9] and Sears[12] have shown that the laminar boundary on a swept infinite wing may be determined in a simple manner. Outside the boundary layer in the inviscid region, the flow is obtained by superposition of a two-dimensional flow perpendicular to the wing leading edge (chordwise flow) and a spanwise flow parallel to the leading edge with a velocity V_0. The chordwise velocity component U outside the boundary layer is given as a function of x from two-dimensional potential flow theory z is the coordinate in the spanwise direction; i.e., in the direction of the towline axis.

The boundary-layer problem becomes soluble after recognizing that any quantity, inside as well as outside the boundary layer is independent of z. Let us consider the case of vanishing chordwise flow. In a purely spanwise flow, we would expect a growth of the boundary layer in the z direction and thus dependence on z. Actually, we must exclude the special case of vanishing chordwise flow; if the chordwise flow exists, it will remove fluid contained in the spanwise layer so that a constant thickness exists in the z direction, and thus, independence of z becomes possible. The spanwise component of the velocity in the boundary layer v then becomes a function of x alone. Once this is recognized, it may be concluded that the chordwise flow may be calculated as if no spanwise flow were present.

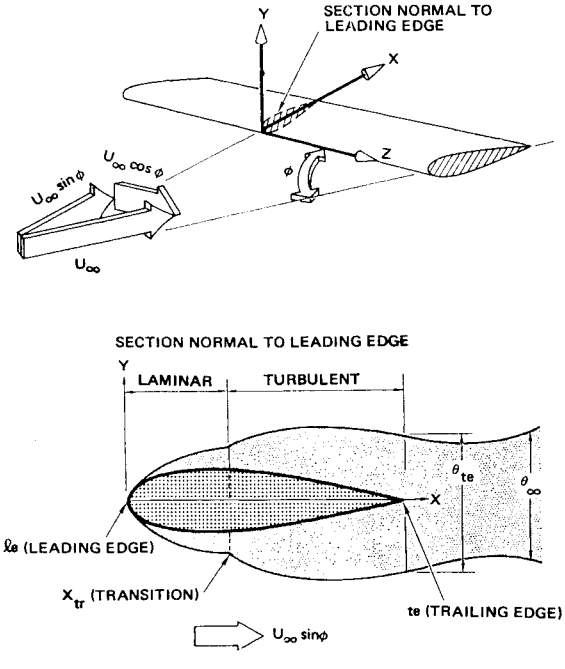

Fig. 4 Coordinate system.

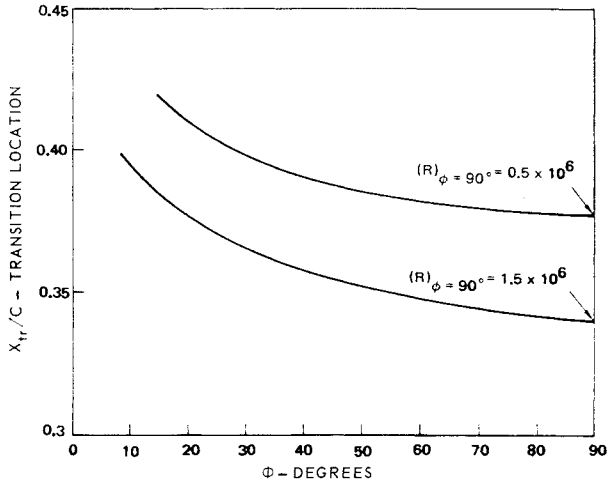

Fig. 6 Boundary-layer transition location.

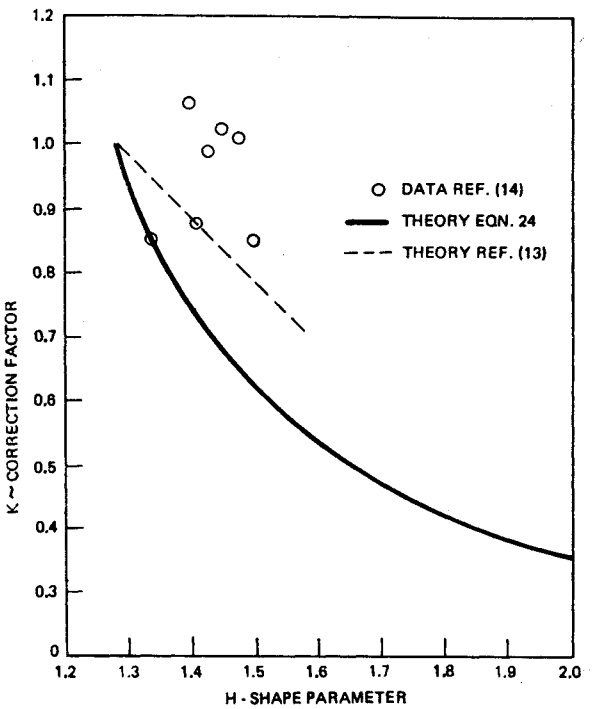

Fig. 7 Mixed-momentum thickness correction factor.

It was theorized by Young and Booth[13] and supported by experimental evidence for a flat plate that the "Independence Principle" for yawed infinite wings is also valid for the turbulent boundary layer. Altman and Hayter[14] gave further experimental evidence in support of this theory for the case of a swept wing (at zero lift) in turbulent flow. Further discussion by Rott and Crabtree[15] give credibility to the Independence Principle.

Use of the Independence Principle, in essence, means that in the case of the faired towline, the normal force is composed of pressure forces (determined solely by the chordwise velocity component) and frictional forces, while the tangential force is the result only of frictional stresses due to the spanwise velocity component.

4.1 Normal Loading Function—$L(\phi)$

Based on the Independence Principle, the normal loading function is developed as follows:

$$U_0 = U_\infty \sin\phi \tag{8}$$

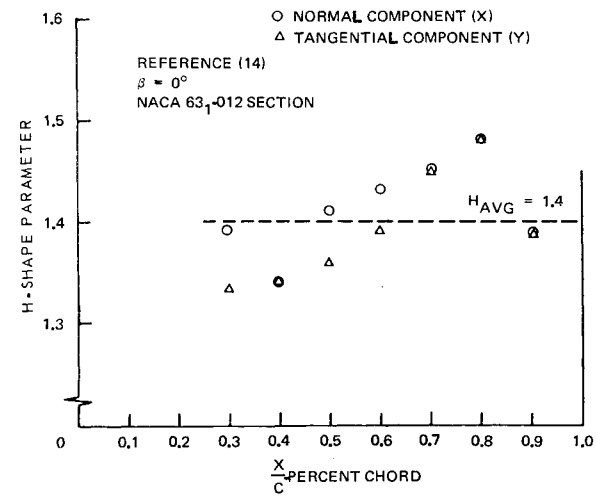

Fig. 8 Comparison of shape parameter H for swept wing based on the X and Y components of velocity.

$$Re(\phi) = Re(\phi = 90°) \sin\phi = (U_\infty c/\nu) \sin\phi \tag{9}$$

Using the data from Fig. 5, curves of boundary-layer transition location as a function of towline angle ϕ for constant values of $Re(\phi = 90°)$ may be developed as shown in Fig. 6.

The total normal force at a given towline angle is thus,

$$F(\phi) = C_R(\phi)\rho U_0^2 S/2 = C_R(\phi)(\rho U_\infty^2/2) \sin^2\phi S \tag{10}$$

where $C_R(\phi)$ is developed from Eq. (7) using Fig. 6. The nondimensional normal loading function is

$$\frac{F(\phi)}{R} = \frac{C_R(\phi)\rho U_\infty^2 \sin^2\phi S_{\frac{1}{2}}^2}{C_R(\phi = 90°)\rho U_\infty^2 S_{\frac{1}{2}}^2} = \frac{C_R(\phi)\sin^2\phi}{C_R(\phi = 90°)} \tag{11}$$

4.2 Tangential Loading Function—$G(\phi)$

Since, as assumed, the towline section is constant along its length, the tangential force $G(\phi)$ has no form or pressure drag component and is strictly the result of the shearing stress τ_{yz}. The tangential force $G(\phi)$ per unit length is

$$G(\phi) = \int_0^c (\tau_{yz})dx \tag{12}$$

where

$$\tau_{yz} = \rho V_0^2 \left(\frac{\partial\theta_{zx}}{\partial x}\right)dx \tag{13}$$

so that

$$G(\phi) = \rho V_0^2 \int_0^c \left(\frac{\partial\theta_{zx}}{\partial x}\right)dx = \rho V_0^2 [\theta_{zx}]_{le}^{te} \tag{14}$$

The θ_{zx} is assumed to vary from zero at the leading edge le to $(\theta_{zx})_{te}$ at the trailing edge te where

$$\theta_{zx} = \int_0^\delta \frac{u}{V}\left[1 - \frac{u}{V}\right]dy = \frac{U}{V}\int_0^\delta \frac{u}{U}\left[1 - \frac{v}{V}\right]dy \tag{15}$$

or θ_{zx} may be expressed in terms of the total momentum

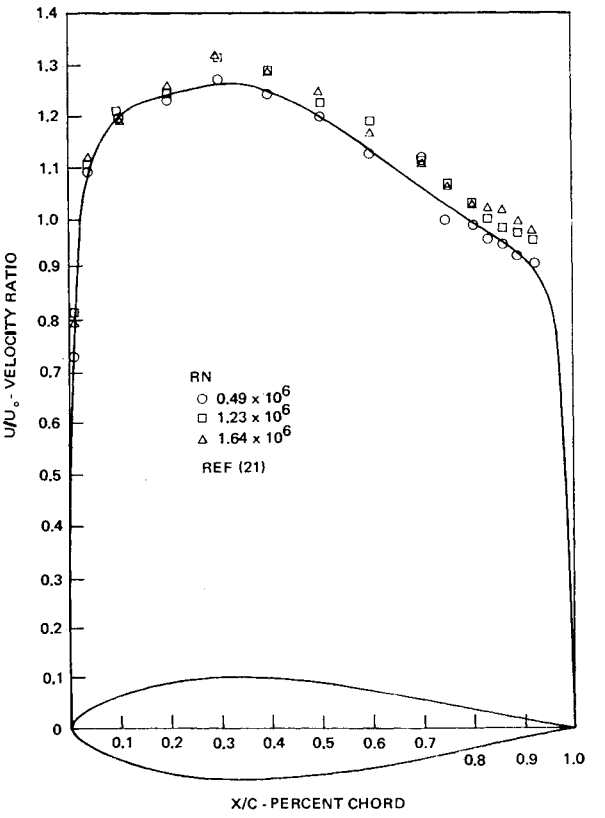

Fig. 9 63A020 section-velocity ratio.

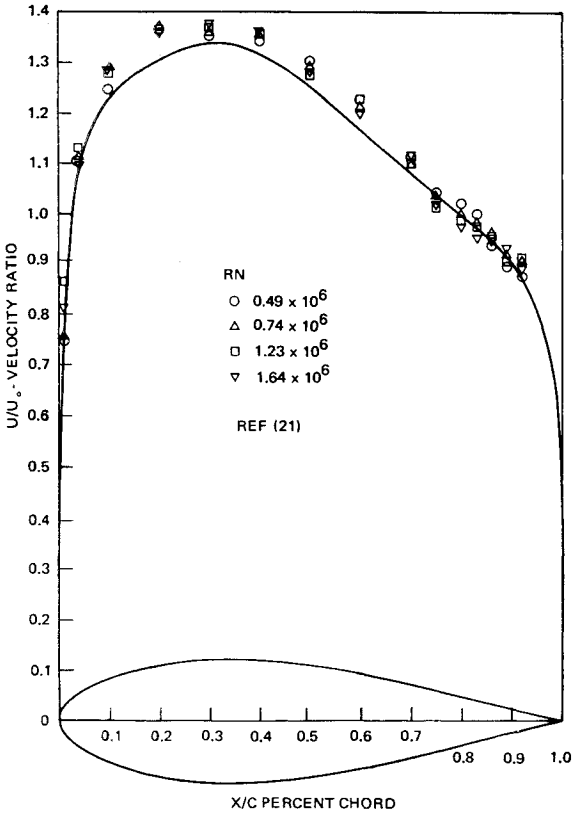

Fig. 10 63A025 section-velocity ratio.

thickness θ_{te} at the trailing edge

$$\theta_{zz} = (U_{te}/V_0)K\theta_{te} \tag{16}$$

where

$$K = \frac{1}{\theta_{te}}\int_0^{\delta}\frac{u}{U}\left[1 - \frac{v}{V}\right]dy \tag{17}$$

Under the assumption of a turbulent boundary layer at the trailing edge K may be determined if the following assumptions are made: 1) the distribution of v/V_0 is the same for any x where the boundary layer is turbulent, and is independent of the chordwise pressure gradient and 2) $v/V_0 = (y/\delta)^{1/7}$ as for a flat plate in turbulent flow. Now since

$$\frac{u}{U} = \left[\frac{y}{\delta}\right]^{(H_{te}-1)/2} = \left[\frac{y}{\delta}\right]^{n};\quad n = \frac{H_{te} - 1}{2} \tag{18}$$

then

$$K = \frac{\delta}{\theta_{te}}\int_0^1\left[\frac{y}{\delta}\right]^n\left[1 - \left(\frac{y}{\delta}\right)^{1/7}\right]d\left(\frac{y}{\delta}\right) = \frac{\delta}{\theta_{te}}\left[\frac{1}{n+1} - \frac{1}{n+1+\frac{1}{7}}\right] \tag{19}$$

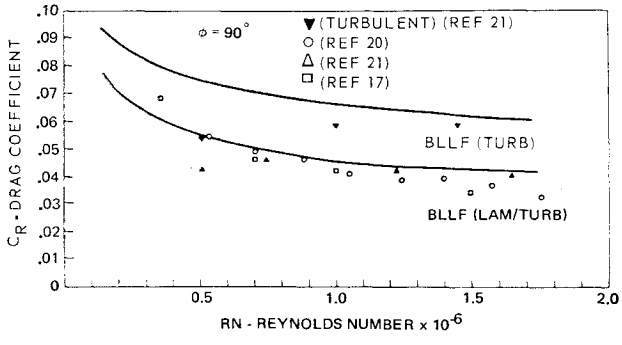

Fig. 11 63A022 section-drag coefficient.

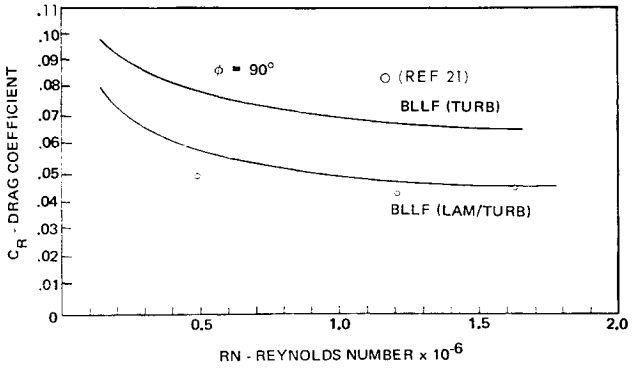

Fig. 12 63A020 section-drag coefficient.

since

$$\frac{\delta}{\theta_{te}} = \frac{(n+1)(2n+1)}{n} \tag{20}$$

then

$$K = \left[\frac{\frac{1}{7}}{n}\right]\left[\frac{2n+1}{1+n+\frac{1}{7}}\right] = \frac{4H_{te}}{7H_{te}^2 + 2H_{te} - 9} \tag{21}$$

A comparison of experimentally determined values of K (Ref. 14) with those computed from Eq. (21) are shown in Fig. 7. The value of K was also computed by using the method of Ref. 13.

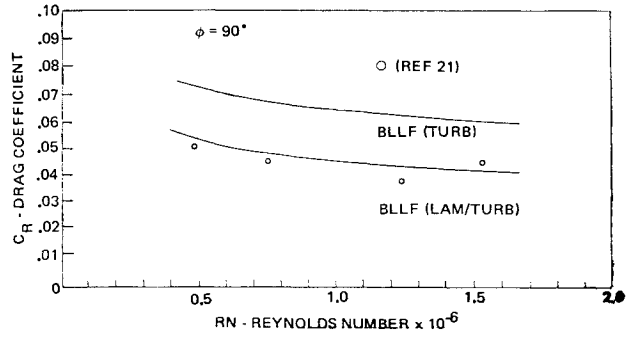

Fig. 13 63A025 section-drag coefficient.

Reference 14 also provides experimentally determined values of H(Fig. 8) derived from velocity profiles measured in the normal and tangential directions on the surface of a swept airfoil section. An average value of 1.4 was chosen as a representative value to be used for H_{te}. K, as determined by Eq. (21), is thus 0.745.

Now the tangential force may be expressed as

$$G(\phi) = \rho V_0^2(U_{te}/V_0)K\theta_{te} = \rho V_0 U_{te}K\theta_{te} \tag{22}$$

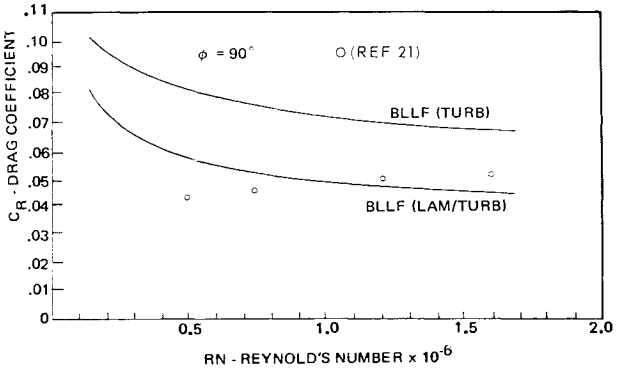

Fig. 14 0020 section-drag coefficient.

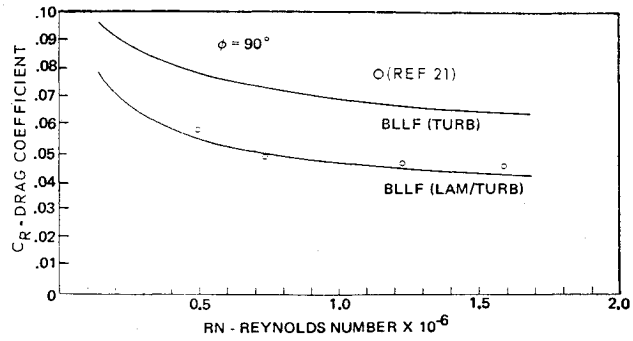

Fig. 15 0022 section-drag coefficient.

However, from Eqs. (2) and (6)

$$\theta_{te} = [F(\phi)/\rho U_0^2][U_0/U_{te}]^{(Hte + 5)/2} \quad (23)$$

where $F(\phi)$ is substituted for R so that $G(\phi)$ may be expressed in final form as

$$G(\phi) = \rho V_0 U_{te} K[F(\phi)/\rho\, U_0^2]\,[U_0/U_{te}]^{(Hte + 5)/2} =$$
$$KF(\phi)[U_\infty \cos\phi/U_\infty \sin\phi][U_{te}/U_0][U_0/U_{te}]^{(Hte + 5)/2} =$$
$$KF(\phi)\cos\phi\ [U/U_0]_{te}^{(Hte + 3)/2} \quad (24)$$

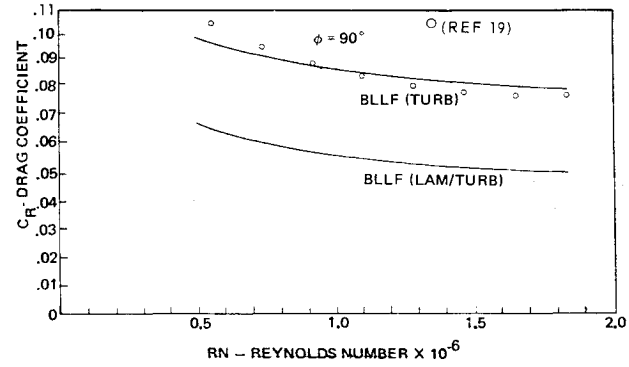

Fig. 16 AEW section-drag coefficient.

and

$$G(\phi)/R = (F(\phi)/R)\{K\cot\phi[U/U_0]_{te}^{(Hte + 3)/2}\} \quad (25)$$

Using

$$H_{te} = 1.4 \text{ and } K = 0.745$$
$$G(\phi) = 0.745F(\phi)\cot\phi[U/U_0]_{te}^{2.2} \quad (26)$$
$$G(\phi)/R = [F(\phi)/R][0.745\cot\phi(U/U_0)_{te}^{2.2}] \quad (27)$$

The velocity ratio at the trailing edge deserves some comment. From potential theory, $(U/U_0)_{te}$ has a value of zero.

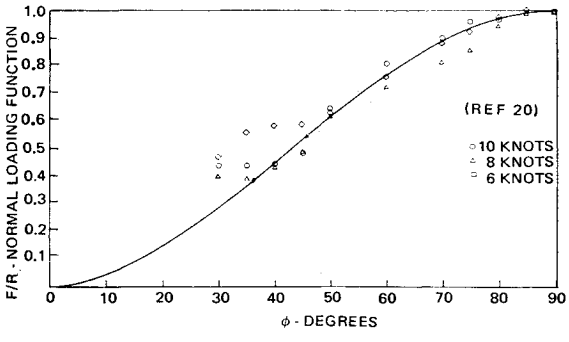

Fig. 17 63AO22 section-normal loading function.

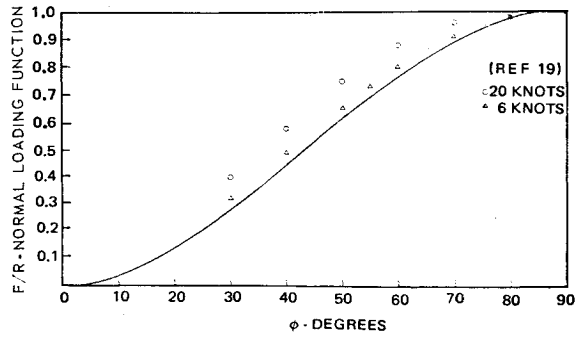

Fig. 18 AEW section-normal loading function.

This of course is not realized in practice, as full pressure recovery is never achieved. An approximation was made by assuming that the velocity ratio $(U/U_0)_{te}$ is equal to the value obtained by extending the slope of the aft portion of the velocity ratio curve to the trailing edge.

5.0 Comparison with Experimental Data

Data from four different sources were used to verify the proposed theory. These were NACA wind-tunnel data Refs. 16–18, AEW tow tank data (Ref. 19), tow tank data (Ref. 20), and Hydronautics water channel data (Ref. 21). The comparison is divided first into the normal drag coefficient as a function of Reynolds number, and then nondimensional loading functions, $F(\phi)/R$ and $G(\phi)/R$.

In addition, Hydronautics[21] made pressure measurements over the surface of two NACA airfoil sections, the NACA 63A020 and 63A025. Figures 9 and 10 provide a comparison with the potential theory computations made using the Weber[6] method. The data show excellent agreement with the theory.

5.1 Normal Force Comparison

Figures 11–16 show the data and theory comparisons for the NACA 63A022, 63A020, 63A025, 0020, 0022, and AEW sections, respectively.

Theoretical values for full turbulent flow and for combined laminar and turbulent flow were computed for each case. The drag coefficients are based on the projected frontal area rather than planform area as is common in airfoil work.

It was expected that the NACA 63A series would experience some degree of laminar flow. This appears to be indicated by the excellent agreement between the data and the laminar/turbulent line for the NACA sections (Figs. 11–13).

The NACA 4 digit series sections showed similar results. Figures 14 and 15 indicate that the 0020 and 0022 sections experienced some degree of laminar flow as evidenced by the correlation with the laminar/turbulent curve.

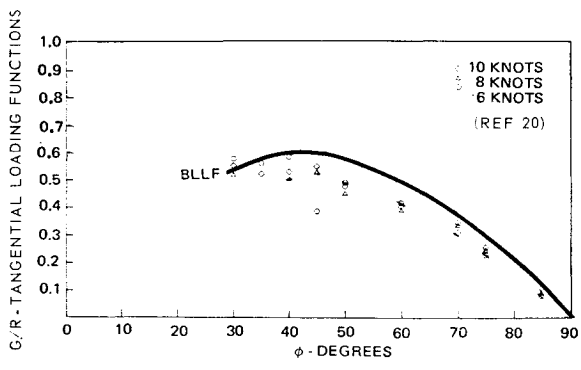

Fig. 19 63AO22 section-tangential loading function.

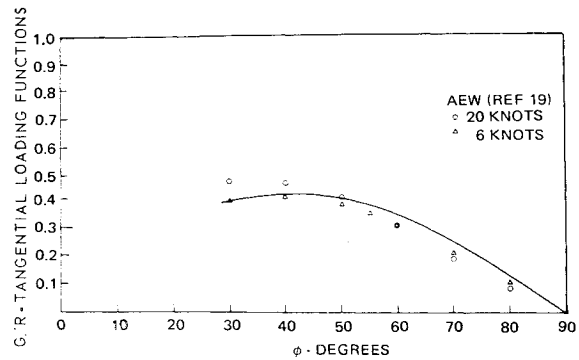

Fig. 20 AEW section-tangential loading function.

The AEW section showed different results. Because of the rather blunt forebody, a large pressure peak exists near the leading edge. It is expected that this should cause transition to turbulent flow very near to the leading edge. Figure 16 shows that the data do agree closely with the full turbulent line.

5.2 Loading Function Comparison

The nondimensional loading functions $F(\phi)/R$ and $G(\phi)/R$ are shown in Figs. 17–20 for the NACA 63A022 and AEN sections.

The normal loading function data shows good agreement for the NACA 63A022 section down to a towline angle of about 40°. The data then tend to lie slightly above the theoretical line. The data for the AEW section lie above the theoretical line over the full angle range down to the minimum angle of 30°. The nondimensional tangential loading function data show excellent agreement for both sections with the theory over the full angle range down to 30°.

6.0 Conclusions

A case has been made for a theoretical approach to faired towline hydrodynamics based on boundary-layer considerations. Comparison with available experimental data indicates good engineering agreement. The method thus allows the designer to develop the hydrodynamics of the faired towline with knowledge of only the section coordinates, the chord length, and the speed.

References

[1] Eames, M. C., "Steady-State Theory of Towing," Rept. W6(1967), The Royal Institution of Naval Architects, London.

[2] Clark, J. W., "Extension of Underwater Towing Cable Theory to High Speeds," Rept. B1101128-1, Sept. 1963, United Aircraft Corp., East Hartford, Conn.

[3] Whicker, L. F., "The Oscillatory Motion of Cable-towed Bodies," Ph.D. thesis, July 16, 1957, University of California, Berkeley, Calif.

[4] Squire, H. B. and Young, A. D., "The Calculation of the Profile Drag of Aerofoils," Repts. and Memo No. 1838, Nov. 1937, Royal Aircraft Establishment.

[5] Thwaites, B., "Incompressible Aerodynamics," Clarendon Press, Oxford, 1960, p. 181.

[6] Weber, J., "The Calculation of the Pressure Distribution Over the Surface of Two-Dimensional and Swept Wings with Symmetrical Aerofoil Sections," Rept. AERO 2497, Royal Aircraft Establishment.

[7] Gregory, N., Stuart, J. T., and Walker, W. S., "On the Stability of Three-Dimensional Boundary Layers with Applications to the Flow Due to a Rotating Disk," *Philosophical Transactions*, No. 248, Aerodynamics Div., National Physical Lab., pp. 155–199.

[8] Silverstein, A. and Becker, J. V., "Determination of Boundary-Layer Transition of Three Symmetrical Airfoils in the NACA Full-Scale Wind Tunnel," Rept. 637, NACA.

[9] Jones, R. T., "Wing Plan Forms for High Speed Flight," TR 863, NACA.

[10] Lippisch, A. and Beuschausen, W., "Pressure Distribution Measurements at High Speed and Oblique Incidence of Flow," Tech. Memo No. 1115, March 1947, NACA.

[11] Dannenberg, R. E., "Measurements of Section Characteristics of a 45° Swept Wing Spanning a Rectangular Low Speed Wind Tunnel as Affected by the Tunnel Walls," TN 2160, Aug. 1950, NACA.

[12] Sears, W. R., "The Boundary Layer of Yawed Cylinders," *Journal of Aeronautical Sciences*, Vol 15, No. 1, Jan. 1948, pp. 49–52.

[13] Young, A. D. and Booth, T. B., "The Profile Drag of Yawed Wings of Infinite Span," *Aeronautical Quarterly*, Vol. 3, Nov. 1951.

[14] Altman, J. M. and Hayter, N. F., "A Comparison of the Turbulent Boundary-Layer Growth on an Unswept and a Swept Wing," TN 2500, Sept. 1951, NACA.

[15] Rott, N. and Crabtree, L. F., "Simplified Laminar Boundary-Layer Calculations for Bodies of Revolution and for Yawed Wings," *Journal of the Aeronautical Sciences*, Vol. 19, 1952.

[16] Abbott, I. H. and Von Doenhoff, A. E., "Theory of Wing Sections," Dover, New York, 1949.

[17] Jacobs, E. N. and Abbott, I. H., "Airfoil Section Data Obtained in the NACA Variable-Density Tunnel as Affected by Support Interference and Other Corrections," TR 669, 1939, NACA.

[18] Loftin, L. K., Jr. and Smith, H. A., "Aerodynamic Characteristics of 15 N.A.C.A. Airfoil Sections at Seven Reynold's Numbers from 0.7×10^6 to 9.0×10^6," TN 1945, Oct. 1949, NACA.

[19] Lofft, R. F., "Resistance and Lift of Cable Fairing when Inclined to Direction of Flow," Admiralty experiment works, 1958.

[20] Unpublished Test Report on Experimental Loading Functions for NACA 63A022 Airfoil Section, Towing Tank Tests.

[21] Etter, R. J. and Haung, T. T., "An Experimental Investigation of the Static Hydrodynamic Characteristics of Several Simulated Faired Cables Having Symmetrical NACA Airfoil Sections," TR 530-1, July 1967, Hydronautics Inc., Laurel, Md.